Nanostructured WC_x/CNTs as highly efficient support of electrocatalysts with low Pt loading for oxygen reduction reaction

Changhai Liang,*[a] Ling Ding,[a] Chuang Li,[a] Min Pang,[a] Dangsheng Su,[b] Wenzhen Li[c] and Yuemin Wang[d]

Received 21st January 2010, Accepted 9th April 2010
DOI: 10.1039/c001423k

Highly active Pt–WC_x/carbon nanotube (CNT) electrocatalysts for the oxygen reduction reaction (ORR) have been developed by the combination of tungsten carbide with CNTs as electrocatalyst supports. The obtained WC_x/CNT and Pt–WC_x/CNT samples were characterized by XRD, TEM, XPS and electrochemical measurements. The results showed that nanostructured tungsten carbide particles on carbon nanotubes could be prepared by microwave-assisted thermolytic molecular precursor method, and the particle size of tungsten carbide increased with the increase of tungsten loading. The nanostructured WC_x/CNTs showed electrocatalytic activity for oxygen reduction reaction. The deposition of Pt nanoparticles on the WC_x/CNTs resulted in higher electrocatalytic activity for the oxygen reduction reaction and better immunity to methanol than Pt/CNT catalysts. The unique electrocatalytic properties of the novel Pt–WC_x/CNT electrocatalyst were attributed to a synergistic effect between Pt, WC_x and the CNTs. The findings also indicated that WC_x/CNTs were efficient electrocatalyst supports that could reduce Pt usage while the same electrocatalytic properties were kept for the ORR in direct methanol fuel cells.

1. Introduction

Direct methanol fuel cells (DMFC), a kind of polymer electrolyte fuel cells, are attracting much more attention for their potential as electrical power sources for vehicles, stationary and portable applications due to their high energy density, easier storage and distribution than that of liquid methanol at ambient conditions.[1,2] The oxygen reduction reaction (ORR) is an important electrochemical reaction involved in proton exchange membrane fuel cells.[3,4] However, the low reaction rate of the ORR and the prohibitive production cost in Pt-based electrocatalysts are the main problems.[5–7] Moreover, methanol crossover from the anode to the cathode leads to an extra loss in the overall efficiency of direct methanol fuel cells. Therefore, current research is aimed to develop cost effective and methanol tolerant catalysts which should increase the reaction rate of the ORR and reduce the Pt loadings.

To enhance the activity of the ORR and decrease the cost of the electrocatalysts, one strategy is to explore highly active catalysts with novel support materials, since the support materials of catalysts play an important role in the dispersion of metal nanoparticles and the transportation of reactants/products, which directly influence the catalytic activity and stability of catalysts.[8–11] Tungsten carbides as electrocatalyst supports have shown an important promotion effect for ORRs in DMFC, due to their interactions with Pt and reactivity towards the hydrogen peroxide intermediate.[12–14] The recent research has revealed that tungsten carbides can be employed as highly efficient supports of electrocatalysts to facilitate methanol oxidation in DMFC.[15]

[a]*State Key Laboratory of Fine Chemicals and Key Laboratory for Micro/Nano Technology and System of Liaoning Province, Dalian University of Technology, China. E-mail: changhai@dlut.edu.cn; Fax: + 86 411 39893991; Tel: +86 411 39608806*
[b]*Department of Inorganic Chemistry, Fritz Haber Institute of the Max Planck Society, Germany*
[c]*Department of Chemical Engineering, Michigan Technological University, USA*
[d]*Chair of Physical Chemistry I, Ruhr-University Bochum, Germany*

Broader context

Direct methanol fuel cells are attracting much more attention for their potential as electrical power sources for vehicles, stationary and portable applications due to their high energy density, easier storage and distribution of liquid methanol at ambient conditions. The low rate of oxygen reduction reaction and the prohibitive production cost in Pt-based electrocatalysts are the main problems. Moreover, methanol crossover from the anode to the cathode leads to an extra loss in the overall efficiency of direct methanol fuel cells. Herein, nanostructured tungsten carbides were combined with carbon nanotubes as electrocatalyst supports for improving the activity of oxygen reduction reaction and reducing Pt loadings. Highly uniform and well dispersed nanostructured tungsten carbide particles of about 2–5 nm on carbon nanotubes have been successfully prepared by thermolytic molecular precursor method under microwave irradiation. The obtained Pt–WC_x/CNTs showed much higher electrocatalytic activity for oxygen reduction reaction than Pt/CNT catalysts under the same conditions, and a unique immunity to methanol. The findings indicated that WC_x/CNTs as efficient electrocatalyst supports could reduce Pt usage while the same electrocatalytic properties were kept for the oxygen reduction reaction in direct methanol fuel cells.

Moreover, tungsten carbides are very stable in acidic solutions, which efficiently prevents Pt from falling off the support, and have good electrical conductivity. However, preparation of interstitial carbides with nanostructure and/or high surface area is very difficult by the conventional methods, which have been inherited from the metallurgical industry at high temperature, and are energy-intensive – thus resulting in large grains of low surface area. Although a variety of chemical and physical preparative methods have been developed, the controlled synthesis of nanostructured carbides, *i.e.* below the particle size of 5 nm, still remains a big challenge for electrocatalyst applications.[16–21] Recently, carbon nanotubes (CNTs) had been used as electrocatalyst supports for DMFC and showed an enhancement effect on the catalytic activity of the ORR[22–24] due to their unique structure and properties. Here we combined tungsten carbides with CNTs as electrocatalyst supports for improving the activity of the ORR and reducing Pt loadings. Highly uniform and well dispersed nanostructured tungsten carbide particles of about 2–5 nm on CNTs have been successfully prepared by thermolytic molecular precursor method under microwave irradiation, and show different electrocatalytic activity from the low surface area material. The obtained Pt–WC_x/CNTs showed much higher electrocatalytic activity for ORRs than Pt/CNT catalysts under the same conditions, and a unique immunity to methanol.

2. Experimental

2.1 Preparation of WC_x/CNTs and Pt–WC_x/CNTs

Nanostructured WC_x/CNTs were prepared by thermolytic molecular precursor method under microwave irradiation at atmospheric pressure. The preparation details of the WC_x/CNT samples can be found elsewhere.[25] In brief, The WC_x/CNTs were synthesized from CNTs and tungsten hexacarbonyl by mixing in an agate mortar for 0.5 h. The completely homogeneous precursor mixture was put in a quartz-tube reactor and heated for 30 min by a microwave oven operating at 2.45 GHz with a power of 800 W.

The Pt–WC_x/CNT electrocatalysts were then prepared by a modified ethylene glycol method. 0.072 g of dihydrogen hexachloroplatinic acid was dissolved in about 100 ml of ethylene glycol. The pH value was adjusted to above 10 through the addition of a 1.0 M NaOH in ethylene glycol. Then after the solution was heated under reflux to 160 °C for 3 h, 0.02 g of the as-prepared WC_x/CNT sample was added and the pH value was slowly brought down to 2 by the dropwise addition of an aqueous solution of 0.1 M HCl. Then the mixture was heated to 160 °C again and kept for 1.5 h to deposit Pt colloids onto the WC_x/CNTs. The whole preparation process was conducted under flowing argon. After cooling to room temperature, washing and drying, the Pt–WC_x/CNT electrocatalyst was obtained. For comparison, a Pt/CNT sample with the same metallic Pt loading was also prepared by the ethylene glycol method.[22,24]

2.2 Characterizations

X-Ray diffraction (XRD) analysis of the samples was carried out using a Rigaku D/Max-RB diffractometer with Cu Kα monochromatized radiation source ($\lambda = 1.54178$ Å), operated at 40 kV and 100 mA.

Transmission electron microscopy (TEM) was performed using a Philips CM200 FEG transmission electron microscope (accelerating voltage 200 kV) using high-resolution imaging and energy-dispersive X-ray spectroscopy (EDX). The composition distribution analysis with a resolution of a few nanometres was performed in the STEM mode in combination with energy dispersive X-ray spectroscopy (EDX) using a DX4 analyzer system (EDAX) in the same microscope.

The high resolution XPS measurements were carried out in an ultra-high vacuum (UHV) set-up equipped with the Gamma-data-Scienta SES 2002 analyzer. Monochromatic Al Kα (1486.6 eV) X-ray source was used as incident radiation. The base pressure in the measurement chamber was 2×10^{-10} mbar. The analyzer slit was set to 0.4 mm and a pass energy of 200 eV was chosen, resulting in an overall energy resolution better than 0.5 eV. Charging effects were compensated by the usage of a flood gun. The binding energies were calibrated based on the graphite C 1s peak at 284.5 eV as a reference. The XPS peaks are analyzed using a Shirley-type background and a nonlinear least-squares fitting of the experimental data based on a mixed Gaussian/Lorentzian peak shape.

2.3 Measurement of electrochemical properties

A CHI 760B potentistat/galvanostat was used for the electrochemical measurements in a standard three-compartment electrochemical cell with a glassy carbon working electrode. A Pt-foil and a saturated calomel reference electrode (SCE) were used as the auxiliary and reference electrode, respectively. Cyclic voltammetry (CV) experiments were carried out at 25 °C in 0.5 M H_2SO_4 solution. About 5 mg catalyst was ultrasonically suspended with 2 mL of ethanol and 50 μL of 5 wt% Nafion solution for 15 min, then about 20 μL suspension was spread on the clean glass carbon electrode and dried to obtain a thin active layer. Before each measurement, fast potential pulses (100 mV s^{-1}) between 0 and 1400 mV were applied to the electrodes for surface cleaning and for obtaining a reproducible active electrochemical surface. The electrochemical surface area (ECSA) of the Pt–WC_x/CNT catalyst was determined by integrating the hydrogen adsorption/desorption areas of the cyclic voltammogram (assuming 210 μC cm^{-2} Pt after double layer correction) obtained in a potential pulse at a scan rate of 50 mV s^{-1}. The potential was then cycled at 25 mV s^{-1} starting at −0.24 V for two complete oxidation/reduction cycles.

The activity of the ORR on these catalysts was evaluated on the thin-film rotating disk electrode (Pine Instruments, US). For the thin-film RDE measurements, 20 μL of the well-dispersed catalyst ink, which was prepared in the CV test, was spread onto the clean glass carbon disk, as described in CV tests. ORR activity was measured in oxygen-saturated 0.5 M H_2SO_4 electrolyte at 25 °C with a CHI 760B potentistat/galvanostat. A linear sweep was started from the cathodic direction at a scan rate of 5 mV s^{-1} and the rotating speed was fixed at 1600 rpm. The electrolyte was bubbled with an oxygen flow for about 1 h before each experiment and maintained over the electrolyte during the whole voltammetry measurement.

3. Results and discussion

The WC_x/CNT samples with 4.5, 8.7, 13.2 and 18.4 wt% tungsten loadings were prepared by thermolytic molecular precursor method under microwave irradiation at atmospheric pressure. Tungsten loading was measured by TGA as described in literature.[25] Their XRD patterns were shown in Fig. 1. No diffraction peaks assigned to WC_x phases were observed for the sample with 4.5 wt% tungsten loading, indicating highly dispersed WC_x on the CNTs. XRD pattern of the sample with 8.7 wt% tungsten loading showed three diffraction peaks at 34.5, 39.4, and 62.0°, which could be assigned to W_2C with hexagonal closed-packed structure. At the same time, diffraction peaks at 36.8 and 42.8° were also detected, which were due to tungsten oxycarbide with face-centered cubic structure (JCPDS 22-0959). The results were different from those in literature[26] due to the different method for sample preparation. For the sample with 13.2 wt% tungsten loading, the new diffraction peaks at 31.5, 35.8 and 48.4°, which could be attributed to WC with hexagonal closed-packed structure, were observed besides the diffraction peaks due to W_2C and tungsten oxycarbide. Further increasing tungsten loading to 18.4 wt%, the diffraction peaks became sharper, indicating that WC_x particles grew with the increase of tungsten loading. We had reported that the WC_x particles tended to become larger as the microwave irradiation time increased.[25] This result was different from that obtained by carbothermal hydrogen reduction, where the size of WC_x particles supported on activated carbon with high surface area was independent of the tungsten loading.[20]

In order to investigate the structural property and the composition distribution, TEM and STEM were carried out. The typical TEM images of the samples with 8.7 and 18.4 wt% tungsten loadings arre shown in Fig. 2. It can be seen that the particle size of WC_x was about 3 nm in diameter dispersed on the outer surface of the CNTs for the samples with 8.7 wt% tungsten loadings (Fig. 2a), while the particle size of WC_x was about 5 nm in diameter for the samples with 18.4 wt% tungsten loadings (Fig. 2b), and was larger than that of the samples with 8.7 wt%, which is in agreement with the sizes obtained from XRD. The homogeneous W, C and O distributions in the sample with 18.4 wt% (b) tungsten loading were confirmed by STEM dark field image and the corresponding elemental maps shown in Fig. 3. The existence of O was due to the oxygen-containing groups on CNTs from their purification process by HNO_3 solution and the formation of passivated layers on WC_x particles, which can avoid violent oxidation of the sample when it was exposed in air.

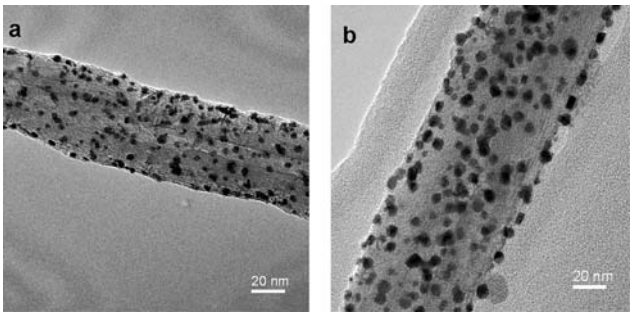

Fig. 2 TEM images of the WC_x/CNTs samples with 8.7 wt% (a) and 18.4 wt% (b) tungsten loading.

Pt–WC_x/CNT and Pt/CNT samples were prepared by the modified ethylene glycol method. Fig. 4 showed XRD patterns of CNT, Pt/CNT and Pt–WC_x/CNT samples with 10.7 wt% Pt loading, together with WC_x/CNT sample with 18.4 wt% tungsten loading. For the Pt/CNT catalyst, the characteristic peaks at 39.6, 46.4 and 67.8° were detected and could be attributed to metallic Pt with face-centred cubic crystalline structure corresponding to (111), (200) and (220), while the diffraction peaks at 26.5 and 43.5° were ascribed to graphite with hexagonal structures. XRD pattern of Pt–WC_x/CNTs combined features of WC_x/CNTs and Pt/CNTs indicated that Pt particles were deposited on the WC_x/CNTs. The mean particle size of the Pt nanoparticles estimated from the Pt (220) peak with the Scherrer equation, was approximately 5.0 nm.

As observed from a typical TEM image in Fig. 5, WC_x and Pt particles were in spherical shape, and no agglomeration was observed. The WC_x and Pt particle sizes in the Pt–WC_x/CNT sample ranged from 2 to 6 nm, which is in good agreement with

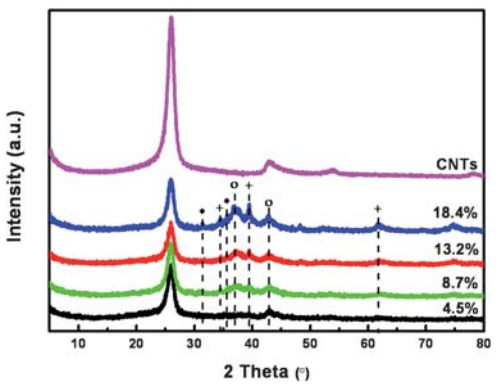

Fig. 1 XRD patterns of CNTs and WC_x/CNTs samples with different tungsten loadings by thermolytic molecular precursor method (* WC, + W_2C, ○ WC_xO_y).

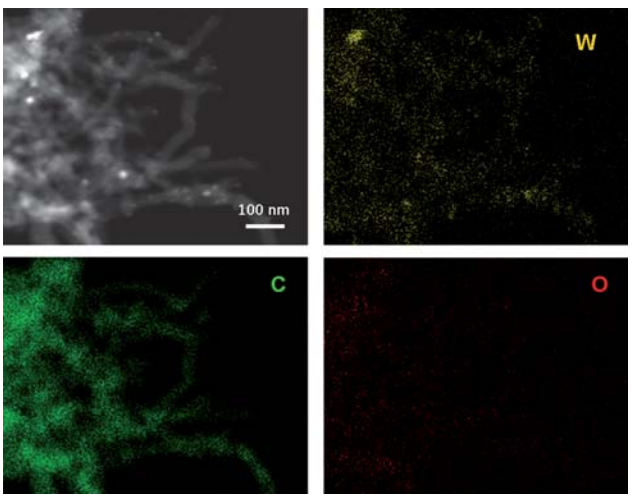

Fig. 3 Representative STEM dark-field images and corresponding X-ray maps of W, C and O for 18.4 wt%WC_x/CNTs.

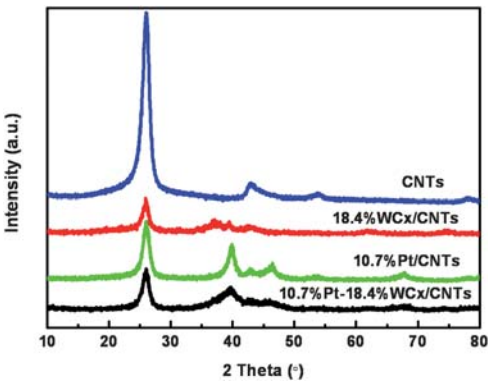

Fig. 4 XRD patterns of CNTs, Pt–WC_x/CNTs, Pt/CNTs and WC_x/CNTs samples.

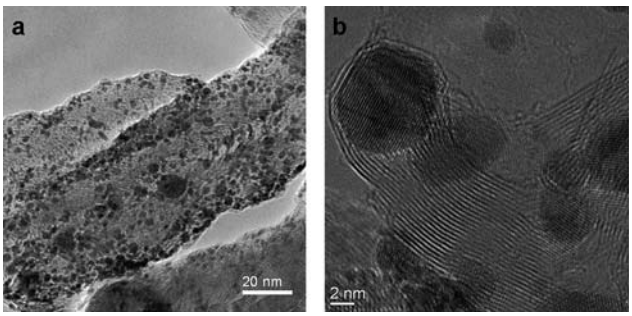

Fig. 5 Representative TEM and HRTEM images of 10.7%Pt–18.4%WC_x/CNT sample.

the XRD results. The particle sizes of Pt on WC_x/CNTs were a little larger than those on the preoxidized CNTs (about 2–4 nm). This was due to the absence of surface groups on the WC_x/CNT support, which have been reported to play an important role on the anchoring metallic particles.[27] The HRTEM image in Fig. 5b further showed that the Pt and WC_x particles in spherical shape overlay mutually on the outer wall of CNTs although it is difficult to identify them due to the similar lattice spacings. The homogeneous WC_x and Pt distributions in the Pt–WC_x/CNT sample were also confirmed by the STEM dark field image and the corresponding elemental maps shown in Fig. 6. The outer walls of the CNTs were uniformly covered by well-dispersed tungsten carbide and Pt throughout the sample without agglomeration. Oxygen in WC_x/CNT remained after Pt nanoparticles were deposited on the support, indicating that the oxygen-containing groups on the CNTs and the oxygen from passivated oxidic layers on WC_x particles were stable in the modified ethylene glycol process.

The surface chemistry of the CNTs, WC_x/CNTs and Pt–WC_x/CNT samples was further studied by high resolution XPS. Fig. 7 shows the corresponding XPS survey spectra. For the raw CNTs, C was obviously observed and nearly no O was detected, indicating that few oxygen-containing groups existed on the CNTs from the purification process by HNO_3 solution. Impurities were not detected in the CNTs. It was found when the preoxidized CNTs were used to prepare the supported tungsten carbide particles by the microwave-assisted thermolytic molecular precursor method, few tungsten carbide particles were

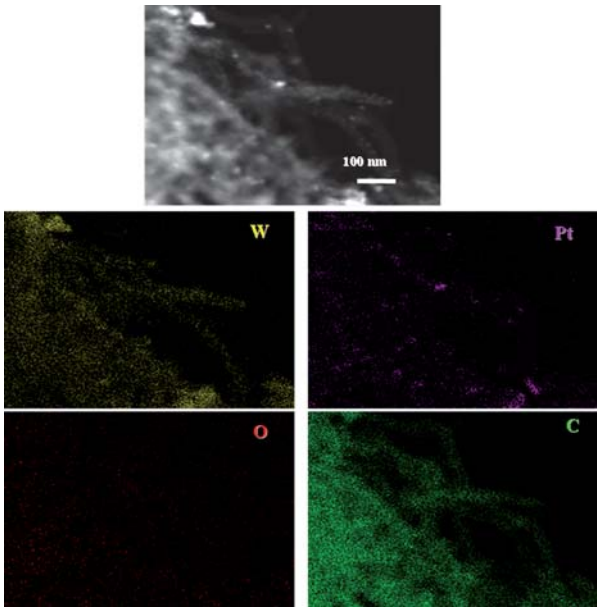

Fig. 6 Representative STEM dark-field images and corresponding X-ray maps of W, Pt and C for 10.7%Pt–18.4%WC_x/CNT sample.

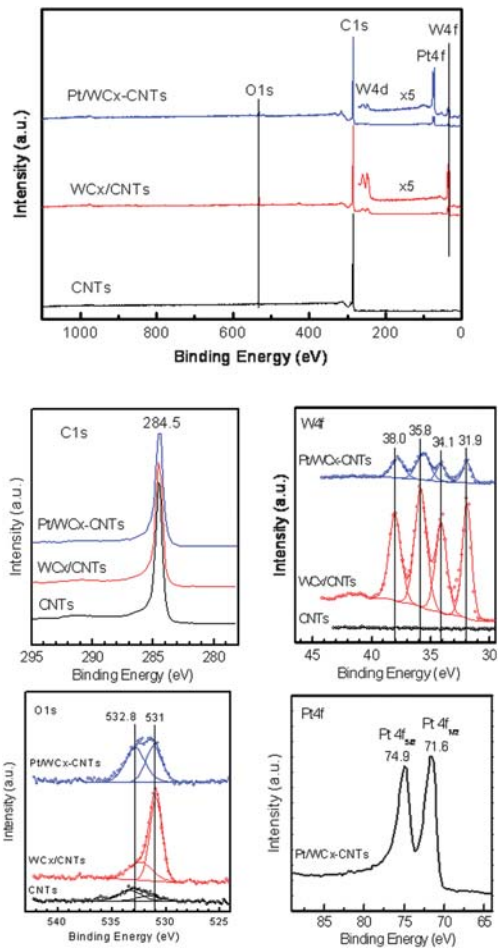

Fig. 7 XPS survey and high resolution spectra of CNTs, 18.4%WC_x/CNTs and 10.7%Pt-18.4%WC_x/CNTs samples.

observed.[25] W, C and O elements were observed in the XPS spectrum of the WC_x/CNT sample. The O 1s peak increased significantly after the WC_x deposition on CNTs, which was consistent with those from XRD and STEM. The Pt 4f peak was observed as well as W, C and O elements in the Pt–WC_x/CNT sample, indicating that Pt particles were deposited on the WC_x/CNTs.

As shown in Fig. 7, the C 1s spectrum at 284.5 eV was assigned to the sp^2 carbon atoms in the three samples, which is consistent with the assignment in literature.[27,28] The W 4f spectra of the WC_x/CNT and Pt–WC_x/CNT samples could be deconvoluted into two doublets ($4f_{7/2}$ and $4f_{5/2}$ peaks). The first doublet of W 4f peaks at 31.9 and 34.1 eV was attributed to WC. The second one observed at 35.8 and 38.0 eV could be assigned to WO_3.[29] The deconvolution of O 1s spectra of the three samples resulted in two peaks: WO_3 at 531.0 eV and O functional groups on the CNTs at 532.8 eV.[27] The Pt 4f spectrum of the Pt–WC_x/CNT sample showed one doublet with Pt $4f_{7/2}$ binding energy of 71.6 eV and Pt $4f_{5/2}$ binding energy of 74.9 eV, which is characteristic of the metallic Pt(0) species. The observed Pt $4f_{7/2}$ binding energy for Pt(0) is slightly higher than that of either bulk platinum ($4f_{7/2}$ = 71.2 eV) or platinized carbon electrodes ($4f_{7/2}$ = 71.2 eV).[30] The positive shift in binding energy corresponds to a decrease in the electronic charge density on the platinum atoms present in the Pt–WC_x/CNTs sample. This might arise from metal–support interactions, where there might be an electron shift from the metal to the WC_x/CNT support.

The ORR activities of the CNT, WC_x/CNT, Pt/CNT and Pt–WC_x/CNT samples in sulfuric acid solution were compared in Fig. 8. Only CNTs had no elelctrocatalytic activity for ORRs, while WC_x/CNTs gave the electrocatalytic activity for ORRs in acidic solution. Tungsten carbide microspheres were reported to be inactive towards ORRs in sulfuric acid solution.[31] However, W_2C/C showed catalytic activity towards ORRs in sulfuric acid solution.[31] To the best of our knowledge, this is the first report on the electrocatalytic activity of WC_x/CNTs for ORRs in sulfuric acid solution. This could be attributed to highly uniform and well dispersed tungsten carbide nanoparticles with 2–5 nm. Both Pt/CNTs and Pt–WC_x/CNTs were much more active than WC_x/CNTs. However, there was a significant difference between their onset potentials. The Pt–WC_x/CNT electrocatalyst was more favorable for the reduction of oxygen by a more positive shift in the onset potential compared to the Pt/CNTs electrocatalyst with the same Pt loading. The oxygen electroreduction on the Pt–WC_x/CNTs is over 50 mV more positive compared to that of the Pt/CNTs. Even with half amount of Pt loading, the Pt–WC_x/CNT electrocatalyst had the more positive onset potential as compared with the Pt/CNT electrocatalyst, indicating that a synergistic effect between Pt, WC_x and the CNTs. What deserves to be highlighted is that the reduction in the amount of Pt is significant in terms of the cost and the resource limitation. The limiting current of the Pt–WC_x/CNT catalyst was significantly larger than that of the Pt/CNT catalyst, which means that more oxygen molecules could reach the surface of the Pt–WC_x/CNT catalyst, which may be due to the larger electrochemical surface area from the smaller particle sizes.

Fig. 9 showed the linear sweep curves of the Pt–WC_x/CNT samples with different WC_x loadings in the O_2 saturated H_2SO_4 solution. By increasing the WC_x loading from 8.7 wt% to 18.4 wt%, the limiting current of the Pt–WC_x/CNTs catalyst increased, However, when the WC_x loading further increases to 26.8 wt%, the limiting current decreases sharply. This means that the amount of oxygen molecules to the surface of the Pt–WC_x/CNT catalyst is also affected by the WC_x loadings, which may be related to particle sizes of the WC_x confirmed by XRD and TEM.

Cyclic voltammograms of the Pt/CNT and Pt–WC_x/CNT electrocatalysts in 0.5 M H_2SO_4 solution at a scan rate of 25 mV s^{-1} are presented in Fig. 10. The CV curve of the Pt/CNT catalyst showed the well-defined hydrogen adsorption-desorption peaks in the potential region of −0.24 to 0.04 V. The formation current of Pt oxide appeared at higher potentials than 0.9 V. This represented typical characteristic features of a polycrystalline Pt electrode. Similar hydrogen adsorption-desorption peaks were also observed for the Pt–WC_x/CNT catalyst, suggesting that Pt particles were dispersed on the WC_x/CNTs. The hydrogen adsorption and desorption areas for Pt/CNTs was smaller than that for Pt–WC_x/CNTs, suggesting that electrochemical active surface area on the Pt/CNT catalysts was lower than that on the Pt–WC_x/CNT catalysts. The double layer area of the Pt/CNT sample was larger than the Pt–WC_x/CNT sample, which means WC_x changed the electrochemical properties of the CNTs, and good interactions occurred between Pt nanoparticles and the WC_x/CNTs. Additionally, it can be observed that the

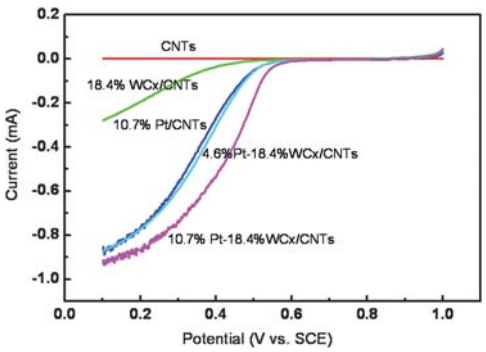

Fig. 8 Linear sweep curves for ORRs on CNTs, WC_x/CNT, Pt/CNT and Pt–WC_x/CNT catalysts in O_2 saturated 0.5 M H_2SO_4 at a scan rate of 5 mV s^{-1} and at 25 °C.

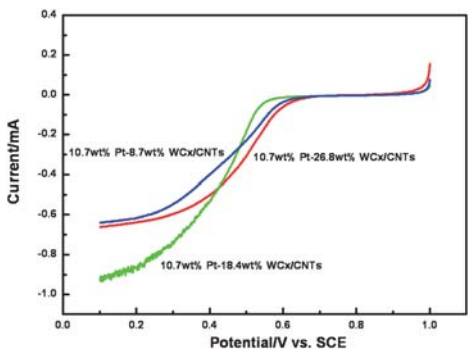

Fig. 9 Linear sweep curves for ORRs on Pt–WC_x/CNT catalysts with different WC_x loading in O_2 saturated 0.5 M H_2SO_4 at a scan rate of 5 mV s^{-1} and at 25 °C.

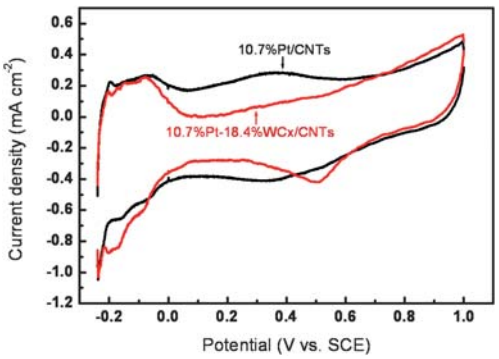

Fig. 10 Cyclic voltammograms of the Pt/CNT and Pt–WC_x/CNT electrocatalysts in 0.5 M H_2SO_4 at a scan rate of 25 mV s^{-1} and at 25 °C.

onset of oxide formation and the peak potential of oxide reduction for Pt–WC_x/CNTs were also shifted to more positive potentials compared with the Pt/CNTs, indicating that the Pt–WC_x/CNTs inhibits the chemisorption of OH on the Pt sites at potentials above 0.6 V. This had a beneficial effect on the oxygen adsorption at low overpotentials, and thus may lead to the enhancement of the ORR kinetics.

Meanwhile, the unique immunity to methanol of the novel Pt–WC_x/CNTs electrocatalyst was also observed as shown in Fig. 11. The ORR on the Pt–WC_x/CNT electrocatalyst was hardly affected by methanol concentration and was still the dominant reaction with the concentration of methanol up to 0.5 M at room temperature. Zhao *et al.* also showed that the

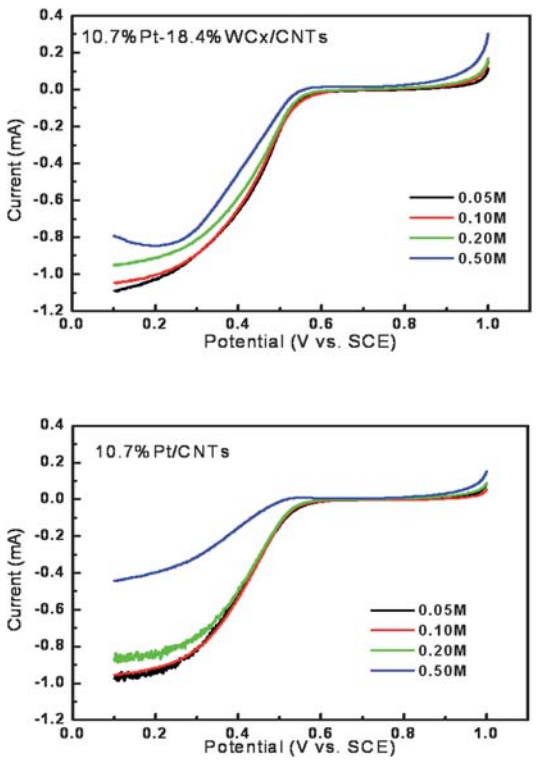

Fig. 11 Linear sweep curves for ORRs on Pt–WC_x/CNTs and Pt/CNTs in O_2 saturated 0.5 M H_2SO_4 with different methanol concentration at a scan rate of 5 mV s^{-1} and at 25 °C.

synergistic effect between Pt nanoparticles and WC could facilitate methanol oxidation,[15] which explains why methanol had little effect on ORR properties of the Pt–WC_x/CNT electrocatalyst. However, it is obvious that the activity for ORRs on the Pt/CNT catalyst was significantly reduced in the presence of methanol with the concentration over 0.5 M. The competitive adsorption of oxygen and methanol on the surface of Pt results in a mixed potential. The electrode reaction was dominant for the methanol oxidation at higher methanol concentration and limited dissolved oxygen, since Pt is active for both oxygen and methanol. The results indicate that the Pt–WC_x/CNTs is a selective electrocatalyst toward oxygen reduction reaction. The unique immunity to methanol of the novel Pt–WC_x/CNT electrocatalyst was attributed to the metal-support interactions, where there might be an electron shift from the metal to the WC_x/CNT support.

4. Conclusions

Evenly distributed nanostructured tungsten carbide particles of about 2–5 nm on CNTs have been successfully prepared by thermolytic molecular precursor method under microwave irradiation. The WC_x/CNT nanocomposites were used as efficient electrocatalyst supports with low Pt loadings for the ORR in direct methanol fuel cells. Introduction of WC_x onto CNTs as a hybrid support for Pt electrocatalysts results in an enhanced activity for the ORR with a more positive onset potential and an increased current density at the same conditions. The Pt–WC_x/CNT catalyst showed a high selectivity for oxygen reduction in the presence of methanol.

Acknowledgements

We gratefully acknowledge the financial support provided by the National Natural Science Foundation of China (No. 20973029), the Scientific and Technical Foundation of Educational Committee of Liaoning Province, and the Scientific Research Foundation for Returned Scholars, Ministry of Education of China.

References

1 S. C. Thomas, X. M. Ren, S. Gottesfeld and P. Zelenay, *Electrochim. Acta*, 2002, **47**, 3741.
2 A. K. Shukla, P. A. Christensen, A. J. Dickinson and A. Hamnett, *J. Power Sources*, 1998, **76**, 54.
3 T. A. Nissinen, Y. Kiros, M. Gasik and M. Leskela, *Chem. Mater.*, 2003, **15**, 4974.
4 H. Meng and P. K. Shen, *J. Phys. Chem. B*, 2005, **109**, 22705.
5 M. R. Tarasevich, A. Sadkowski, E. Yeager, In: B. E. Conway, J. O. M. Bockris,; E. Yeager, S. U. M. Khan, R. E. White (ed.), *Comprehensive Treatise of Electrochemistry*, Plenum Press, New York, 1983, Vol. 7, pp.301–398.
6 R. R. Adzic, In: J. Lipkowski, P. N. Ross (ed.), *Electrocatalysis*, Wiley, New York, 1998, pp.197–242.
7 H. A. Gasteiger, S. S. Kocha, B. Sompalli and F. T. Wagner, *Appl. Catal., B*, 2005, **56**, 9.
8 Y. Y. Shao, J. Liu, Y. Wang and Y. H. Lin, *J. Mater. Chem.*, 2009, **19**, 46.
9 C. A. Bessel, K. Laubernds, N. M. Rodriguez and R. T. K. Baker, *J. Phys. Chem. B*, 2001, **105**, 1115.
10 S. H. Joo, S. J. Choi, I. Oh, J. Kwak, Z. Liu, O. Terasaki and R. Ryoo, *Nature*, 2001, **412**, 169.
11 H. X. Zhong, H. M. Zhang, G. Liu, Y. M. Liang, J. W. Hu and B. L. Yi, *Electrochem. Commun.*, 2006, **8**, 707.

12 M. K. Jeon, H. Daimon, K. R. Lee, A. Nakahara and S. I. Woo, *Electrochem. Commun.*, 2007, **9**, 2692.
13 M. Nie, P. K. Shen and Z. D. Wei, *J. Power Sources*, 2007, **167**, 69.
14 R. Ganesan and J. S. Lee, *Angew. Chem., Int. Ed.*, 2005, **44**, 6557.
15 Z. Zhao, X. Fang, Y. Li, Y. Wang, P. K. Shen, F. Xie and X. Zhang, *Electrochem. Commun.*, 2009, **11**, 290.
16 S. Chouzier, P. Afanasiev, M. Vrinat, T. Cseri and M. Roy-Auberger, *J. Solid State Chem.*, 2006, **179**, 3314.
17 S. V. Pol, V. G. Pol and A. Gedanken, *Adv. Mater.*, 2006, **18**, 2023.
18 J. A. Nelson and M. J. Wagner, *Chem. Mater.*, 2002, **14**, 1639.
19 L. Volpe and M. Bourdart, *J. Solid State Chem.*, 1985, **59**, 348.
20 C. H. Liang, P. L. Ying and C. Li, *Chem. Mater.*, 2002, **14**, 3148; C. H. Liang, F. P. Tian, Z. L. Li, Z. C. Feng, Z. B. Wei and C. Li, *Chem. Mater.*, 2003, **15**, 4846.
21 S. I. Nikitenko, Y. Koltypin, O. Palchik, I. Felner, X. N. Xu and A. Gedanken, *Angew. Chem., Int. Ed.*, 2001, **40**, 4447.
22 W. Z. Li, C. H. Liang, W. J. Zhou, J. S. Qiu, Z. H. Zhou, G. Q. Sun and Q. Xin, *J. Phys. Chem. B*, 2003, **107**, 6292; W. Z. Li, X. Wang, Z. W. Chen, M. Waje and Y. S. Yan, *J. Phys. Chem. B*, 2006, **110**, 15353.
23 G. Wu and B. Q. Xu, *J. Power Sources*, 2007, **174**, 148.
24 V. Selvaraj, M. Alagar and K. Sathish Kumar, *Appl. Catal., B*, 2007, **75**, 129; V. Selvaraj, K. Sathish Kumar and M. Alagar, *J. Colloid Interface Sci.*, 2008, **322**, 537.
25 C. H. Liang, L. Ding, A. Q. Wang, Z. Q. Ma, J. S. Qiu and T. Zhang, *Ind. Eng. Chem. Res.*, 2009, **48**, 3244.
26 T. Kado, *Vacuum*, 2004, **76**, 165.
27 C. H. Liang, W. Xia, M. van den Berg, Y. M. Wang, H. Soltani-Ahmadi, O. Schlüter, R. A. Fischer and M. Muhler, *Chem. Mater.*, 2009, **21**, 2360; S. Kundu, Y. M. Wang, W. Xia and M. Muhler, *J. Phys. Chem. C*, 2008, **112**, 16869; P. Serp and P. Kalck, *Chem. Rev.*, 2002, **102**, 3085.
28 T. I. T. Okpalugo, P. Papakonstantinou, H. Murphy, J. McLaughlin and N. M. D. Brown, *Carbon*, 2005, **43**, 153.
29 A. Katrib, F. Hemming, P. Wehrer, L. Hilaire and G. Maire, *J. Electron Spectrosc. Relat. Phenom.*, 1995, **76**, 195.
30 F. Şen and G. Gökağaç, *J. Phys. Chem. C*, 2007, **111**, 5715.
31 Y. Wang, S. Q. Song, V. Maragou, P. K. Shen and P. Tsiakaras, *Appl. Catal., B*, 2009, **89**, 223; H. Meng and P. K. Shen, *Electrochem. Commun.*, 2006, **8**, 588.